AIAA SciTech Forum
8–12 January 2018, Kissimmee, Florida
2018 AIAA Aerospace Sciences Meeting

10.2514/6.2018-0328

Characterization of RAE 2822 Transonic Airfoil in FSU Polysonic Wind Tunnel Facility

Roopesh Kumar[1], Ross Richardson[2], Jonas Gustavsson[3], Louis Cattafesta[4] and Rajan Kumar[5]
Florida State University, Tallahassee, FL 32310

Zhixiang Liu[6] and Gecheng Zha[7]
University of Miami, Coral Gables, Florida 33124

Wind tunnel tests were carried out to characterize the RAE 2822 supercritical airfoil and implement an active flow control technique. Tests were carried out at various subsonic and transonic Mach numbers and angles of attack. Two load cells connected to the airfoil ends along the quarter chord axis were used to quantify the aerodynamic forces acting on the airfoil. The transonic airfoil was integrated, and the control technique successfully implemented at the Florida State University Polysonic wind tunnel. The paper presents a few preliminary experimental results and describes the lessons learned during the implementation process. Oil flow visualizations revealed the presence of corner vortices on the airfoil suction surface and wedge-like patterns on the lower surface, which indicates a combination of localized regions of transitional and turbulent flow with no shocks or very weak shocks. The measured lift coefficient on the baseline airfoil is much lower than the estimated value based on literature. These results indicate that the airfoil tested need to be modified both regarding its aspect ratio and cross-sectional area to suit the facility. The active flow control technique based on co-flow jet show promise in the improvement of aerodynamic performance.

I. Nomenclature

C – Chord (m)
C_D – Coefficient of drag
C_L – Coefficient of lift
C_M – Coefficient of moment
Cμ - Jet momentum coefficient, $\dot{m}_j V_j / q_\infty S$
M_∞ – Freestream Mach number
$\dot{m}_j$ – Jet mass flow rate (kg/s)
P_∞ - Freestream static pressure (Pa)
q_∞ - Freestream dynamic pressure, $1/2\ \gamma P_\infty M^2_\infty$ (Pa)
Re – Reynolds number
S – Span (m)
V_j – Injected jet velocity (m/s)
α – Angle of attack (degrees)
γ – Ratio of specific heats
μ - Viscosity (kg/(ms))
ρ – Density (kg/m^3)

[1] Graduate Research Assistant, AIAA Student Member
[2] Graduate Research Assistant, Mechanical Engineering
[3] Research Scientist, Mechanical Engineering
[4] University Eminent Scholar and Professor, AIAA Associate Fellow
[5] Associate Professor, AIAA Associate Fellow
[6] Graduate Research Assistant, AIAA Student Member
[7] Professor, AIAA Associate Fellow
*Approved for public release; distribution is unlimited

II. Introduction

TRANSONIC flows over airfoils are characterized by a combination of both subsonic and supersonic flows. For flow over an airfoil at critical Mach number, flow reaches sonic velocities locally over the upper airfoil surface which results in the formation of a shock wave thereby generating a rapid increase in drag. This imposed a speed limitation on aircraft cruise speeds during the mid-20th century. Richard Whitcomb (NASA) designed a supercritical airfoil that exhibited significant performance gains in the transonic regime compared to earlier airfoils. In these supercritical airfoils; a) the upper surface of the airfoil has a substantially reduced curvature, b) a relatively large leading edge radius to expand the flow on the airfoil top surface, c) a camber at the airfoil trailing edge to help with lift recovery, and d) a finite thickness at the trailing edge so that the upper and lower surfaces are parallel to avoid flow separation [1]. The present generation aircraft is designed by default to have supercritical airfoils to operate efficiently at transonic speed, most of the airplanes now cruise at high Mach numbers in the range of 0.8 to 0.9.

In general, most airfoil experimental studies on airfoil are performed at subsonic Mach numbers due to lack of large-scale transonic test facilities at academic institutions. Some significant hurdles to overcome in transonic testing are the tunnel wall effects and the model blockage. Tunnel wall effects can be minimized by using a test model with large aspect ratios, which also helps with a smaller blockage. However, there is a limitation to how small the model can be due to the need to simulate relevant Reynolds numbers and the instrumentation of (such) smaller airfoils is challenging. Increasing the size of the model without giving a thought about blockage effects can lead to chocking of the flow in the test section and improper shock wave pattern on the airfoil surface. Wind tunnels with adaptive wall test sections, ventilated test sections or slotted/perforated wall test sections are used to overcome these problems [2]. Adaptive wall test sections have flexible liners and actuators to change the wall geometry to relieve the flow around the model. Ventilated and slotted/perforated wall test sections have gaps (in them) to ease the flow; they are surrounded by a plenum to keep the system closed. Ventilated walls do not have any moving parts, have simple geometries and cost less than the adaptive wall test sections.

Enhancement of performance at design operating conditions, e.g., extremely short take-off and landings (ESTOL), and at off-design conditions can be achieved using flow control methods. Flow control methods delay the flow conditions that cause a loss of efficiency. There is a range of passive and active flow control methods. Raghunathan [3] provides a review of various passive control technique for shock wave boundary layer interactions (PCSB) that have been used for drag reduction and reducing the shock wave unsteadiness. Some of those methods include the use of bumps, a cavity on airfoil surface, porous surfaces, etc. The application of PCSB at transonic flows was found to improve airfoil stall margin, reduce wave drag and increased lift due to fuller velocity profiles produced downstream of the PCSB. The disadvantage of using PCSB was at low transonic Mach numbers where the profile drag was high. To obtain a net reduction in drag, the freestream Mach number should be large enough such that the reduction in entropy (change magnitude) is higher than the viscous losses. Experimental and numerical studies [4, 5] were aimed at investigating the effectiveness of the DVG's (Dynamic Vortex Generators), where the flow separation is anticipated to deploy the DVG's and retract when the flow is attached. Utilizing such a technique can lead to profile drag reduction at design conditions, and the passive flow control device location is decided considering the shock wave position on the flow surface for a particular Mach number. However, the shock wave position is a function of free stream Mach number and restricts the passive device usage to a single location.

Various active flow control such as tangential blowing at leading edge and trailing edge, pulsed jet separation control and rotating cylinders at the leading edge and trailing edge of the airfoil, etc. have been investigated over a range of conditions. The rotating cylinder technique implemented by Cichy et al. [6] to a low-speed airfoil was found to have an unexpected unstable pitch up characteristics and comes with a penalty of added weight due to mechanical rotating components. The techniques which inject high-speed jets into the main flow like tangential blowing [7] and pulsed jet control [8] would require a jet supply system (e.g., compressor bleed), sensors and complicated actuators which may increase the difficulty of implementation. Zha et al. [9] provide a summary of the critical issues to be considered for active flow control. It should be energy efficient and not cause more energy expenditure. The flow control method used should improve the aerodynamic efficiency which includes a lift enhancement and a drag reduction. Its implementation should be practical and facile. One such promising technology is the co-flow jet (CFJ). In this technique, air flow is sucked near the trailing edge through a suction slot, energized using a pump and then injected near the suction peak parallel to the airfoil surface, thus making it a zero net mass flux technique. This results in energizing the boundary layer and helps the primary flow to overcome the adverse pressure gradient, thereby keeping the flow attached to the airfoil surface even at high angles of attack.

Simulation results [10] indicate that applying CFJ flow control helps in delaying the shock boundary layer interactions on supercritical airfoils and improving circulation. This technique enhances lift and reduces the drag thus improving the overall aerodynamic efficiency. The energy expenditure required to maintain this system is less at higher angles of attack and Mach numbers since the injection is carried out near the suction peak and suction near the trailing edge where the surface static pressure is maximum. The energy expenditure necessary has been quantified numerically, and a trade study of cost vs. benefit for a range of Mach numbers were performed by Lefebvre et al. [11], demonstrating not only the potential for substantial lift enhancement but also an advantage at a low angle of attack cruise conditions. Additional work on the ultimate lift enhancement and cruise efficiency gains of a CFJ airfoil has recently been presented by Yang and Zha [12].

The present experimental study builds on previous work on the RAE airfoil without co-flow by Cook et al. [13] as well as subsonic tests of CFJ airfoils by Wells [14], Kirk [15] and numerical simulations of Zha [10]. The objective of the present experiment was a characterization of the RAE 2822 transonic airfoil using oil flow visualization and force measurements and to implement the CFJ concept on RAE 2822 transonic airfoil. Tests were carried out at various Mach numbers (M=0.5, 0.6 and 0.73) and jet momentum coefficient (Cμ) for flow control at 0 and 2-degree angle of attack. The airfoil and the co-flow jet assembly are explained in the experimental setup section and the oil flow visualization, and load cell quantifications are described in the results section.

III. Experimental Setup

Due to the constraints of a scaled wind-tunnel model, the blowing slot was fed compressed air from a supply system controlled outside the wind tunnel, and the suction slot air was removed using a 450-liter (120 gallons) vacuum tank. To implement CFJ control, the airfoil was modeled to have an aspect ratio of 1.2 and a blockage of 8%.

A. Airfoil Model

The RAE2822 supercritical airfoil utilized in the present test was designed to fit the 0.3048 m (12 inches) width of the FSU/FCAAP Polysonic wind tunnel, being held at both ends of the airfoil by load cells that quantified the aerodynamic forces and moments. Two airfoils were manufactured, one for the baseline case as shown in Fig 1 and one for CFJ flow control (with injection and suction cavities) as shown in Fig 2. The airfoils have a chord length of 0.203 m (8 inches) and a span of 0.302 m (11.9 inches). The internal 3D layout of the CFJ airfoil is shown in Fig 3. The cavities are connected to external supply and suction systems using ¾" NPT pipes.

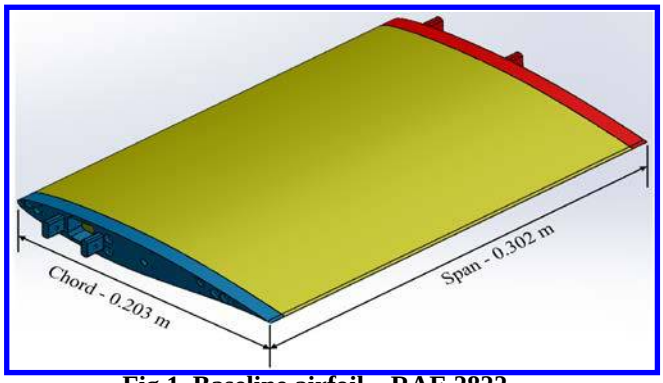

Fig 1. Baseline airfoil – RAE 2822

Fig 2. Cross section of airfoil along mid-span showing two cavities and slots

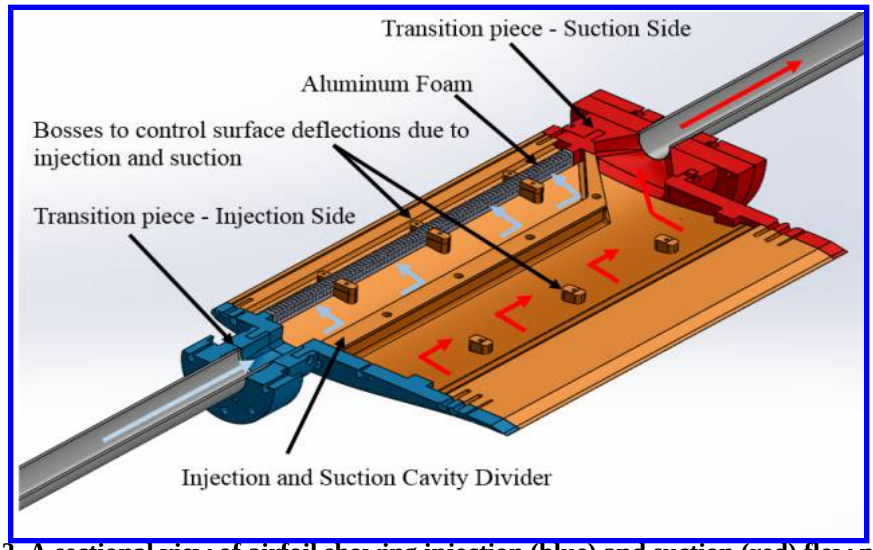

Fig 3. A sectional view of airfoil showing injection (blue) and suction (red) flow paths

To save manufacturing time and cost, the baseline airfoil and the CFJ airfoil were designed in such a way that both airfoils utilize the same assembly. Slot dimensions and design were taken from CFD simulations performed by Zixiang and Zha[15], the injection slot width is 0.6% of chord (located at 0.03C), and the suction slot width is 1.2% of chord (located at 0.75C). The airfoil injection and suction cavities division was decided in such a way that suction cavity would get the maximum cross-sectional area to reduce pressure drop.

The CFJ airfoil was manufactured as two components, the upper and lower segments, which are connected by screws along the cavity divider. Nine bosses (6 for the injection side and 3 for the suction side) were used inside the cavities to connect the upper and lower parts and to minimize the deflection of the airfoil near the injection and suction slots. To build up the pressure inside the injection cavity and get a uniform flow distribution downstream of the injection cavity a Duo-Cell aluminum foam with 35% relative density and 40 pores per inch were utilized.

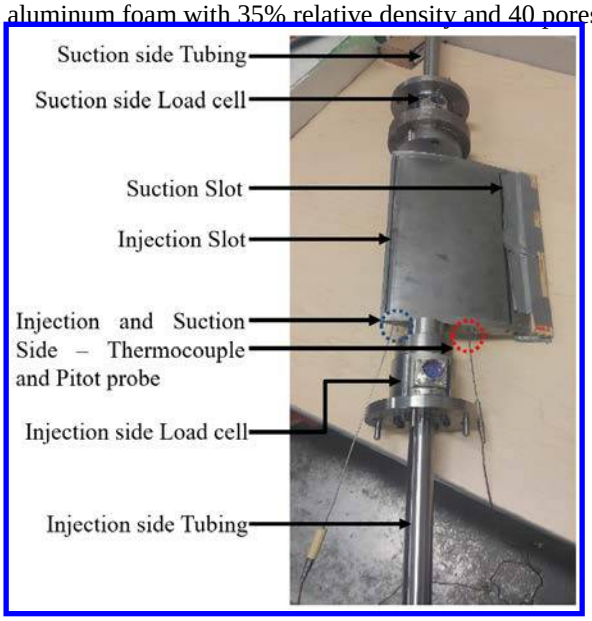

Fig 4. CFJ implemented in the RAE airfoil

B. Airfoil Injection and Suction Assembly

Figs 3 & 4 show the complete airfoil assembly that was mounted inside the wind tunnel for testing. The airfoil has two transitions pieces that change from a circular contour to a rectangular contour. The injection and suction transition pieces were designed to have larger areas than the slots to ensure the flow doesn't choke. To measure the

pressure and temperature inside the injection and suction cavities, K-type thermocouples and pitot probe (connected to a 30 psid ESP) were utilized. A Benchtop test was carried out to examine the flow uniformity of the injection slot. Air from compressed tanks was supplied through the injection tubing while maintaining a constant mass flow for 15 seconds and a pressure transducer was used to measure the pressure distribution along the injection slot. Results indicate that a reasonably uniform flow was exiting the slot with minor pressure variations (less than 5%) along the slot.

C. FSU Polysonic Wind Tunnel

The experiments were carried out in the Polysonic wind tunnel at Florida State University / Florida Center for Advanced Aero-Propulsion (FCAAP). This blow-down facility, shown in Fig. 5, is equipped with sub-, trans- and supersonic test sections of size 0.3048m x 0.3048m (12-inch x 12-inch) and can be used to study flows from Mach 0.2 to 5 and achieve a maximum Reynolds number of 20 million/ft. The sub/supersonic test section is 0.6 m (24-inch) long, and the transonic slotted wall test section is 1.2m (48-inch) long. Run times vary from 60 to 100 seconds depending upon flow conditions. Models can be mounted from sideways using modified plenum windows or using a sting mounted support system which has a pitch control from -10° to 15° and roll control from -180° to 180°. The settling chamber contains an acoustic silencer, 5 flow conditioning screens and a honeycomb structure to minimize the turbulence levels and test section noise. The Polysonic wind tunnel includes an ejector system to reduce the start/stop loads and increase the Reynolds number range, and a plenum evacuation system for shock cancellation and use of higher blockage models at transonic speeds. Current tests focused on the flight envelope of a cargo airplane and were carried out at sub- and transonic speeds, using the transonic test section with the airfoil mounted as shown in Fig 6. Mounting the model inside the test section was done very steadily and cautiously using flanges with push and pull screw arrangements such that the spanwise compressive and tensile forces (Fz) acting on the load cell were minimal.

Fig 5. FSU Polysonic wind tunnel

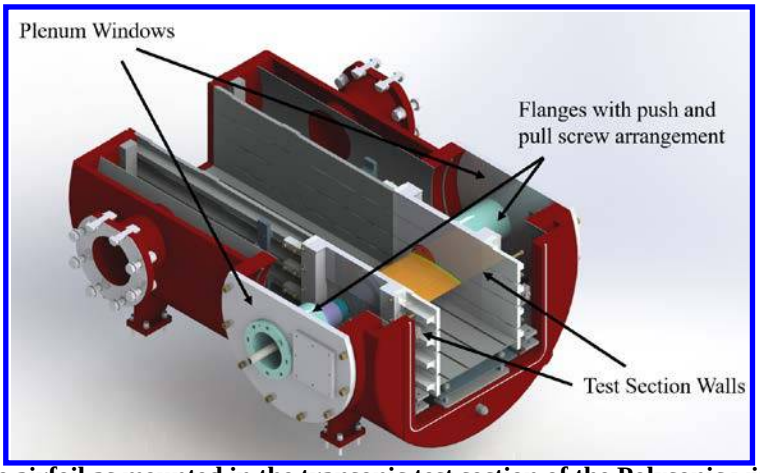

Fig 6. The airfoil as mounted in the transonic test section of the Polysonic wind tunnel

D. CFJ flow control system

A simplified schematic of the open-loop air supply and removal system used for the CFJ airfoil test is shown in Fig 7. As the blow-down wind tunnel only permits short-duration tests and the flow rates required for the test is large, a system with air supplied by two standard 300 cf gas cylinders and a sink consisting of a pre-vacuumed 450-liter (120 gallons) tank was constructed. To control the flow supply, a dome loaded regulator controlled from the wind tunnel control room was employed. Due to the high flow rates and substantial pressure drop between gas cylinder and airfoil, a 2-kW electric heater was required to compensate for the drop in static temperature over the run. The temperatures and pressures of the air were monitored prior to injection into the airfoil. The pressure drop measured before and after the heater was used to determine the injection mass flow rate. On the suction side, both manually controlled ball valve and remotely-controlled pneumatically operated ball valve was used to control the exhaust flow rate. The pressure drop over a calibrated fixed flow restriction was used to measure the flow rate deposited into the vacuum tank. The complete assembly of the CFJ injection (/Supply) and the suction system is shown in Fig 8.

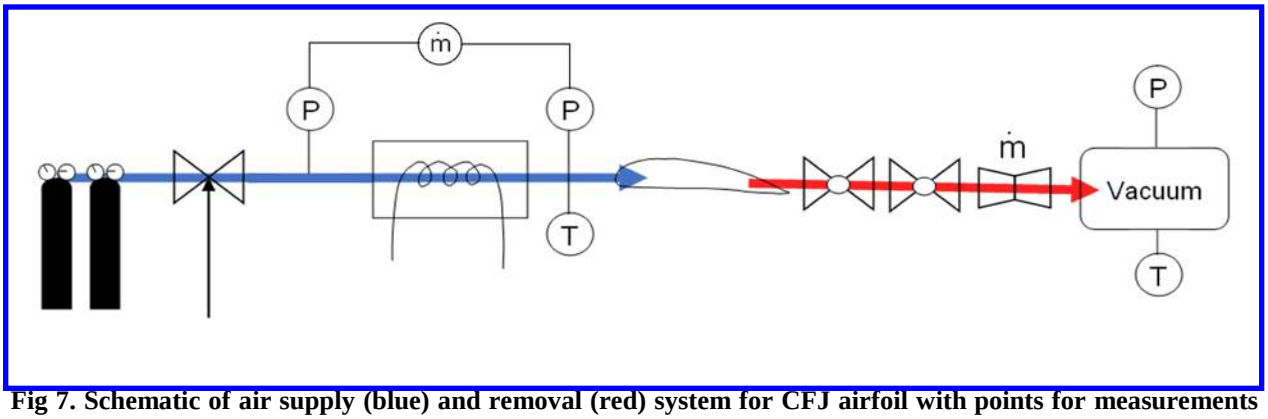

Fig 7. Schematic of air supply (blue) and removal (red) system for CFJ airfoil with points for measurements of mass flow, pressure and temperature indicated.

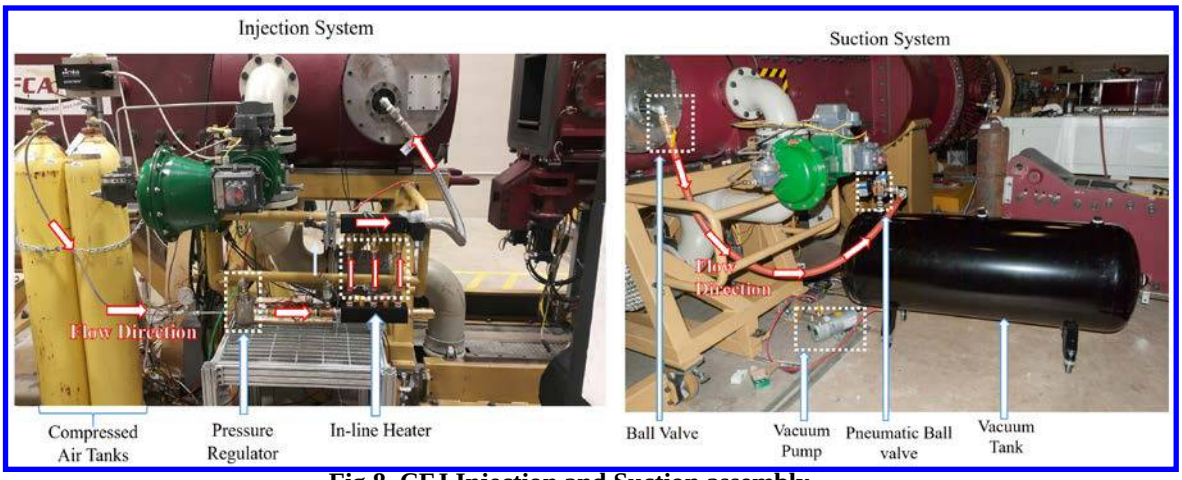

Fig 8. CFJ Injection and Suction assembly.

E. Load Cells

To measure the forces generated by the airfoil, two AMTI AD2.5D-1000 (Fig 4) load cell was used. AD2.5D-1000 is a six-component transducer that measures 3 forces (Fx, Fy, and Fz) and 3 Moments (Mx, My and Mz) with a crosstalk of less than 2%. This load cell's maximum capacity for Fx and Fy is 500 lb, Mz is 500 in-lb, Fz is 1000 lb, and finally, My & Mx are 1000 in-lb. For this experiment Fx, Fy, Mx, and Mz were monitored and measured. Fx gives axial force, Fy – normal force and Mz – Pitching Moment.

The airfoil assembly along with the load cell is connected to the plenum window as shown in Fig 6. This leaves the entire model (to be) suspended in air. This entire system can be simplified as a beam with fixed supports at the ends and the uniformly distributed load acting on it. The normal force acting on the airfoil generates a bending

moment, and Mx component of the load cell was used to monitor this moment. While mounting the airfoil assembly, it was made sure that the airfoil components are affixed directly to the load cell sensing face and do not come into contact with the wind tunnel test section walls. To examine the functioning of the load cell after assembly, weights were placed over the airfoil surface, and the resulting voltages were converted to loads utilizing the calibrated sensitivities. The error between the applied input and the output was less than 1%.

F. Data Acquisition

An NI PXIe-1073 and an SCXI-1000 was used for acquiring data from the control room. Both load-cells was wired to the NI TB-4339 (which was connected to the PXIe-1073) and the SCXI-1314 data card (which was connected to the SCXI-1000). Load cell data was acquired for 5 seconds with a sampling frequency of 960Hz, and the pressure and thermocouple data were acquired with a sampling frequency of 500Hz for 5 seconds.

Before each wind tunnel run, a dry run with no flow condition was performed to check the functioning of the data acquisition system. For the baseline airfoil tests, each test consisted of three sets of data with the first set of data acquired during tunnel start, the second set of data was acquired once the Mach number reached a steady state and the final set of data acquired after the tunnel shut down.

G. Measurement Uncertainties

All measurements have uncertainties no matter how carefully the experiments are carried out. The uncertainty in the tunnel test section Mach number ($0.2 < M < 1.0$) was ±0.005. The pressure transducers used in this experiments Omega PX series and Measurement specialties-30 psid ESP uncertainties are ±0.25% of full scale and ±0.3% of full scale, respectively which yields 0.25 psi for the Omega PX transducers and 0.09 psi for the ESP scanner. The error introduced by the NI PXIe-1073 and SCXI-1000 modules were negligible. The K-Type thermocouples connected to the AD595 amplifier had a maximum error of ±0.05% full scale which was 0.1 ℃. To determine the mass-flow rate uncertainty, the measurement errors in pressure and temperature readings were considered. The maximum error in the calculated mass-flow was ± 5%. For calculating the maximum error in lift, drag and moment, we need to know the uncertainty of the load cell and angle of attack measurements (digital inclinometer was used). Load cells have a maximum error of ±0.2% full scale, and the digital inclinometer max error is ±0.05°. The total uncertainty in aerodynamic forces was calculated using the sum of the squares method, for the lift it was 2.23 lb, for drag it was 1.2 lb and finally 2.33 in-lb for the pitching moment.

IV. Results and Discussions

A. Oil Flow Visualization

The oil flow mixture used consisted of titanium dioxide, oleic acid, and 5W30 motor oil in the ratio of 1:1:4. Oil flow pictures at M=0.73 and an angle of attack of 0 and 2 degrees are shown in Fig 9 and 10. For a zero-degree angle of attack the flow was attached to the airfoil suction surface without any indication of a shock wave, and in the regions more proximate to the sidewalls, the formation of corner vortices could be observed. There was no coagulation of oil on the upper surface to indicate the presence of a shock. The corner vortices developed on both sides of the airfoil could be due to: 1) A minuscule gap (of 0.020 inches) on both sides of the airfoil and test section wall, which was provided to avoid fouling. In this space, the flow moves from a higher pressure region (lower surface) to a lower pressure region (upper surface) thereby generating these corner vortices, and 2) the interaction of sidewall boundary layer with the incoming flow. This may be ascribed as a sidewall boundary layer displacement effect [15]. The lower surface of the airfoil shows wedge-like patterns as seen in Fig 9. Initial thought on the airfoil lower surface flow pattern development was associated with the transonic slotted wall test section suction effect, but another plausible reason for such a pattern was discussed by Norikazu Sudani et al. [15] for a similar supercritical airfoil at 0 degrees angle of attack and M=0.78. In that study, these wedge-like patterns were attributed to the formation of laminar separation bubble terminated by a turbulent reattachment with a very weak shock wave or no shock.

At an angle of attack of 2 degrees similar oil flow patterns are observed, as shown in Fig 10. At $\alpha = 2°$, these wedge patterns are observed on both upper and lower surfaces. Also, an increase in the size of the corner vortices was evident at these conditions.

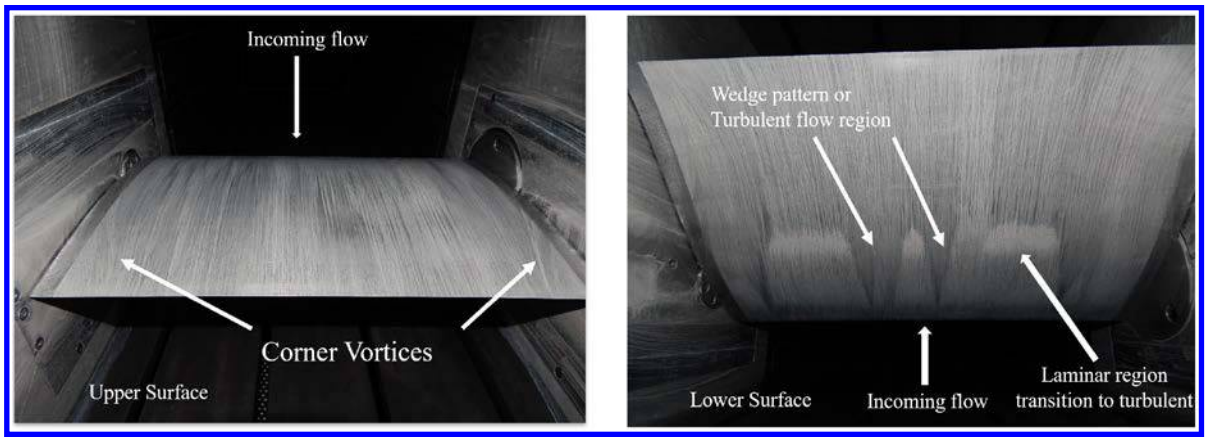

Fig 9. Oil Flow Visualization corresponding to M=0.73 and α = 0.

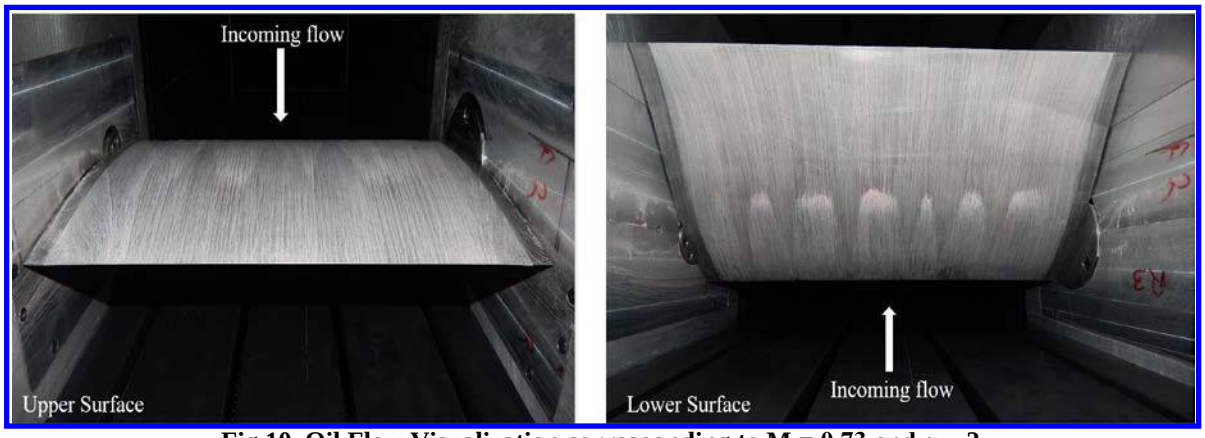

Fig 10. Oil Flow Visualization corresponding to M = 0.73 and α = 2.

B. Aerodynamic Characteristics of the RAE 2822 Airfoil with and without CFJ control

The graph shown in Fig 11 shows a comparison between the lift and drag coefficients for the baseline airfoil and the CFJ airfoil (without any injection or suction) at various Mach numbers. To get the CFJ airfoil without control data, an aluminum foil of 0.0025 inches thick was used to cover the injection and suction slots. At $\alpha = 0°$, the lift coefficient is about 0.08 at Mach 0.5 and increases to about 0.09 at Mach 0.6 and 073. At $\alpha = 2°$ the lift coefficient increases to about 0.2 at all the three Mach numbers. These values of lift coefficient are much lower than the expected levels estimated based on literature and numerical simulations. Comparing the present experimental results with existing research work on RAE 2822 show that the coefficient of lift values are about 70% lower, and the coefficient of drag values are about 30% higher than the previous 2D airfoil data [14], but there wasn't any appreciable difference in the aerodynamic center location. The aerodynamic center (X_{ac}) at M=0.73 calculated from the present experimental results is at 0.27 from the leading edge and 0.26 in numerical simulations by Zha et al. [14]. This questionable difference in the aerodynamic coefficients is may be due to the three-dimensional nature of the flow over the airfoil as evident from the oil flow visualizations. These results suggest that the airfoil need to be modified both in terms of its aspect ratio as well as the frontal area. The two baseline airfoils show nearly identical values of lift coefficient at all the three Mach numbers. The drag coefficient increases with an increase in Mach number. The CFJ baseline airfoil show about 20% higher drag than the clean airfoil which may be due to the aluminum tapes used to cover the injection and suction slots.

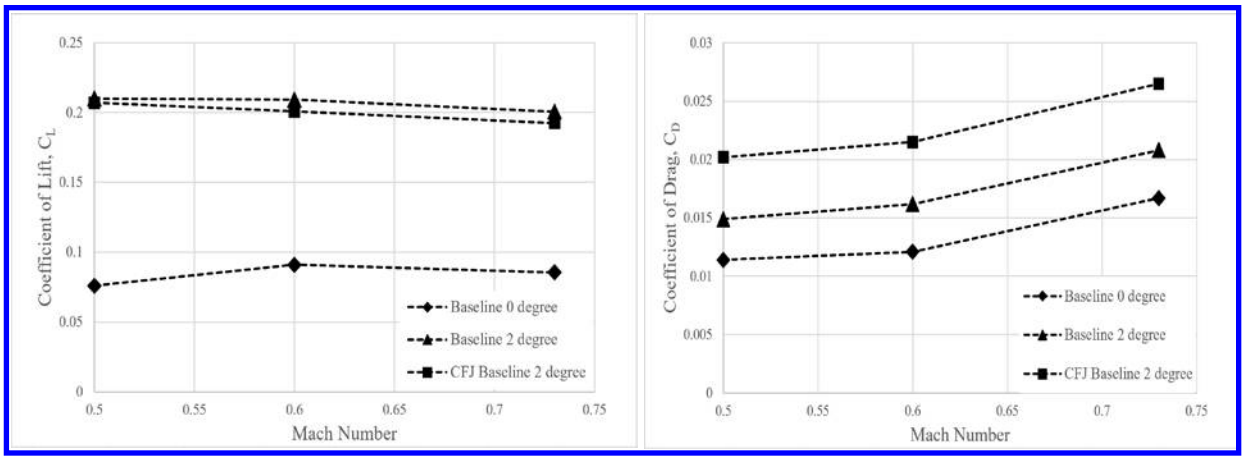

Fig 11. Variations of lift and drag coefficient with Mach number for baseline and CFJ airfoil

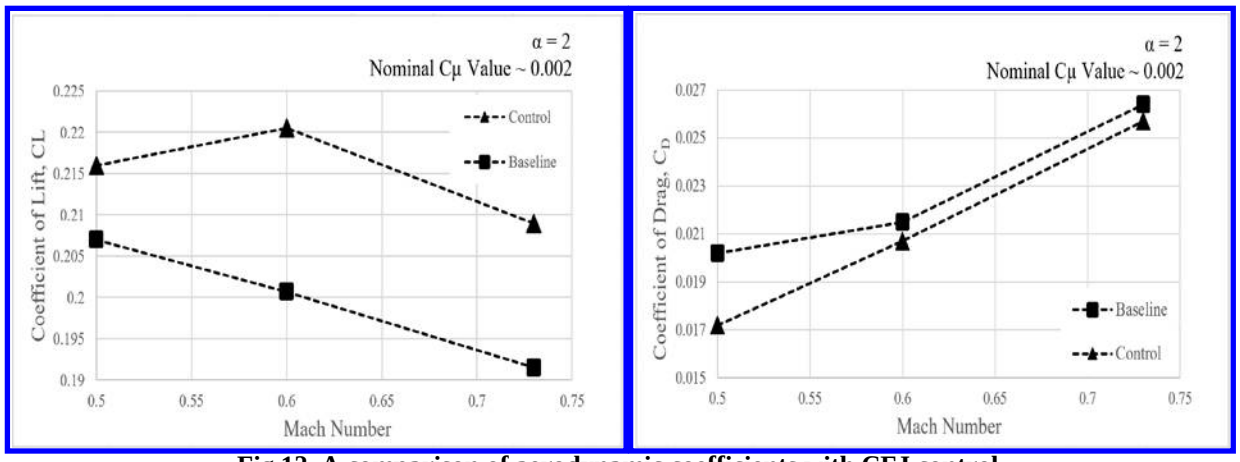

Fig 12. A comparison of aerodynamic coefficients with CFJ control.

Figure 12 shows the effect of CFJ flow control on the lift and drag characteristics of RAE 2822 airfoil at $\alpha = 2°$ over the range of Mach numbers tested. Although a range of momentum coefficient (Cμ) was tested, we here present a case for a nominal Cμ value of 0.002 which corresponds to a mass flow rate of 80 g/s. The results show a significant increase in lift and decrease in drag as compared to baseline airfoil (without control) at all the three Mach numbers. The maximum increase in lift coefficient is about 8%, and the maximum decrease in drag coefficient is 9%. This improvement in aerodynamic performance is likely due to the removal of the low energy fluid near trailing edge and energization of the boundary layer due to injection of a high momentum jet near the suction peak. This flow control mechanism improves the circulation around the airfoil and results in an overall increment in aerodynamic efficiency (L/D) of 10%.

V. Conclusion

The present research work was focused towards characterization of RAE 2822 airfoil and implementation of CFJ flow control concept to the supercritical airfoil in the FSU Polysonic wind-tunnel facility. Oil flow visualizations revealed the presence of corner vortices due to flow moving from high-pressure region to low-pressure region through the test section sidewall and airfoil model clearance and due to the sidewall boundary layer interactions with the incoming flow. Aerodynamic data was acquired for the baseline airfoil and the CFJ airfoil (with and without control) at various Mach numbers (0.5, 0.6 and 0.73) at 0 and 2-degree angle of attack. The present study shows relatively lower lift and higher drag than the nominal 2D baseline airfoil due to the low aspect ratio, higher blockage, and corner vortices. However, the flow control based on CFJ technique shows promise in terms of

increase in lift and a decrease in drag. The current study does not reveal the actual mechanisms responsible for this improvement in aerodynamic performance. Therefore, we plan to design and test a relatively larger aspect ratio and lower blockage airfoil in the future.

VI. Acknowledgments

This project is sponsored by the Defense Advanced Research Projects Agency and monitored by the program manager Dr. Jean-Charles Ledé. The content of the information does not necessarily reflect the position or the policy of the government, and no official endorsement should be inferred. The machining assistance of Texas A&M University, Advanced Concepts Manufacturing, FCAAP machinists Robert Avant and Adam Piotrowski as well as the assistance of the wind tunnel engineers John Strike and Alex Karns in design and test execution is also gratefully acknowledged.

VII. References

[1] Whitcomb, Richard.T, "Review of NASA Supercritical Airfoils," International Council of the Aeronautical Sciences Congress Conference, Haifa, Israel, Aug. 25-30, 1974.
[2] Meyer, Oliver & Nitsche, Wolfgang., "Update on progress in adaptive wind tunnel wall technology," Progress in Aerospace Sciences. 40. 119-141. 10.1016/j.paerosci.2004.02.001.
[3] Raghunathan, S., "Passive Control of Shock-Boundary Layer Interactions" Prog. Aerospace Science, Volume 25, Issue 3, 1988, Pages 271-296.
[4] Rice, Thomas T., Cummings, Reed., Clingman, Dan J., Sahni, Onkar., Amitay, Michael., "Experimental and Numerical Investigation of Static and Dynamic Vortex Generators on an Airfoil with a Deflected Flap," AIAA 2016-4087.
[5] Cummings, Reed., Clingman, Dan., and Sahni, Onkar., "Interactions of a dynamic vortex generator with a cross-flow: A numerical study." AIAA-2015-2482, June 2015.
doi: 10.2514/6.2015-2482.
[6] Cichy, D., Harris, J., and MacKay, J., "Flight Tests of a Rotating Cylinder Flap on a North American Rockwell YOV-10A Aircraft." NASA CR-2135, 1972.
[7] Wood, N., and Robert, L., "Control of Vortical Lift on Delta Wings by Tangential Leading-Edge Blowing," Journal of Aircraft, vol. 25, pp. 236-243, 1988.
[8] McManus, K., and Magill, J., "Airfoil Performance Enhancement Using Pulsed Jet Separation Control." AIAA Paper 97-1971, 1997.
[9] Zha, G.-C., Bruce F. Carroll, Paxton, C., Clark A. Conley and Wells, Adam., "High-Performance Airfoil Using Co-Flow Jet Flow Control," AIAA Journal, Vol. 45, No. 8, pp.2087-2090, 2007.
[10] Zixiang, Liu., Ge-Cheng, Zha., "Transonic Airfoil Performance Enhancement Using Co-Flow Jet Active Flow Control," AIAA Paper 2016-3066, AIAA Aviation 2016/8th AIAA Flow Control Conference, Washington, DC, June 13-17, 2016.
[11] Lefebvre, A., Dano, B., Bartow, W. B., Fronzo, M. D., Zha, G. C., "Performance and Energy Expenditure of Coflow Jet Airfoil with Variation of Mach Number," Journal of Aircraft, 53 (6), 2016.
[12] Yang, Y., Zha, G. C., "Super-Lift Coefficient of Active Flow Control Airfoil: What is the Limit?" AIAA 2017-1693, 55th AIAA Aerospace Sciences Meeting, Grapevine, TX, Jan 9-13, 2017.
[13] Cook, P.H., McDonald, M. A., Firmin, M.C.P., "Airfoil RAE 2822 - Pressure Distributions, and Boundary Layer and Wake Measurements," Experimental Data Base for Computer Program Assessment, AGARD Report AR 138, 1979.
[14] Wells, A.W., "Experimental Investigation of an Airfoil with Co-Flow Jet Flow Control," M.S. Thesis, University of Florida, 2005.
[15] Kirk D., "Experimental and Numerical Investigation of a High-Performance Co-Flow Jet Airfoil," M.S. Thesis, University of Miami, 2009.